

Prediction of Consolidated Sand Dune Erosion by Waves

E. Leone^{a,*}, N. Kobayashi^b, F. D'Alessandro^c and G.R. Tomasicchio^a

^a Department of Engineering for Innovation, University of Salento, EUMER Campus Ecotekne, Lecce, Italy

^b Center for Applied Coastal Research, University of Delaware, Newark, DE, USA

^c Department of Environmental Science and Policy, University of Milan, Milano, Italy

*Corresponding author: elisa.leone@unisalento.it

ABSTRACT

A cross-shore numerical model and laboratory data have been integrated to predict the erosion processes of consolidated sand dunes under irregular breaking waves. The complicated interactions of waves and consolidated sand have been simplified and incorporated into an existing cross-shore numerical model. Natural sand is moved by turbulence generated by wave energy dissipation caused by wave breaking and bottom friction. The addition of a consolidating material injected into the sand limits the movement of the sand particles, increasing the resistance and, consequently, reducing the erosion rate. For the limited erosion case, the resistance parameter of the consolidated sand has been estimated analytically. The erosion model, incorporated into the cross-shore numerical model, has been calibrated with laboratory observations on a small-scale model consisting of a horizontal consolidated sand bottom under non-breaking regular and irregular waves. The calibrated model has been used to simulate the erosion process on a small-scale beach-dune system under breaking irregular waves. The computed profile elevation changes have been found to be consistent with laboratory observations. The results of the numerical simulations confirm the increase in resistance due to the addition of the consolidating material injected into the sand. The numerical model may be used to quantify the benefit of reinforcement a vulnerable sand dune against storms.

KEYWORDS

Coastal Erosion, Sand Dune, Sediment Transport, Colloidal nanosilica, Numerical Modelling.

1 INTRODUCTION

Coastal erosion phenomena at many coastal sites are caused by natural effects largely intensified due to human activities. The integration of traditional and innovative techniques, based on natural processes to create a resilient system, appears to be one of the most promising methods for coastal defense (Foti et al., 2020). Coastal dunes are recognized for their capabilities to prevent coastal flooding during wave storms (D'Alessandro and Tomasicchio, 2016; Tomasicchio et al., 2011). A number of laboratory experiments have been conducted for the investigation and verification of different techniques aiming at coastal dune erosion reduction (e.g., Kobayashi et al. (2013); Leone et al. (2021)). Available experimental data are used to integrate existing numerical models for cross-shore morphodynamics of the beach-dune system and extend their applications. Sediment transport models are used in order to gain insight into the medium- and long-term changes of a coastal system. However, sediment transport modelling is challenging essentially because no dynamic equation is available to describe the movement of a large number of sediment particles. Moreover, transport modeling of sediment mixture containing both loose and consolidated sand is not established yet because the consolidated sand is eroded slowly in comparison to the erosion process of loose sand. As a consequence, sediment transport models are essentially empirical and dependent on reliable experimental data. Nairn and Southgate (1993) developed, and validated with laboratory data, a numerical model to reproduce offshore bar formation on a thin sand layer overlaying a cohesive till substrate. Kobayashi and Weitzner (2015) developed a dike erosion model to predict the temporal and cross-shore variations of vertical erosion depth on the seaward clay slope with or without a turf cover. The dike erosion model was incorporated in the cross-shore numerical model CSHORE (Kobayashi, 2016). Kobayashi and Zhu (2020) used the dike erosion model to predict the erosion of a consolidated cohesive bottom containing cohesionless sediment and compute till profile evolutions for durations of 100–200h. In the present study, CSHORE has been extended to predict the erosion of consolidated sand

using the model of a consolidated cohesive bottom containing cohesionless sediment. The extended CSHORE has been compared with the laboratory data obtained by Leone et al. (2021). The calibrated CSHORE has then been used to compute profile evolutions of a beach-dune system with consolidated sand. In the following, the experiments are briefly described. The extended numerical model and comparison with laboratory observations are discussed in detail.

2 EXPERIMENTS

Physical model tests have been conducted in the 2D wave flume at the EUMER lab, Campus Ecotekne (Lecce, IT). The flume is 45 m long, 1.5 m wide, and 2 m deep equipped with a single paddle wave generator and an active wave absorption system. The experiments have been focused on the verification of an innovative and environmental-friendly technique for the consolidation of coastal sand dunes using a mineral colloidal silica-based grout (D'Alessandro et al., 2020). The experimental campaign is described in detail in Leone et al. (2021). The additive to consolidate the sand consists of a nature-based and non-toxic aqueous suspension with dispersed nanometric particles of colloidal silica (Todaro, 2021). Before injecting nanosilica into the sand, an activator, i.e., a solution of sodium chloride (10 NaCl in water), has been added to the suspension, inducing the mixture to become a gel. Then, the dispersion of the nanosilica-based grout has been carried out by a pressure pulverizer at 20 C, penetrating into the surface layer of the sand. The amount of the grout has been calculated so as to achieve a homogeneous consolidated sand layer of about 5 cm. After spraying the grout and after the completion of the gelling time, a homogeneous consolidation of the sand has been observed. The result consisted of a pore-filling process and an increase in cohesion of the sand; nevertheless, the nanosilica-based material did not interfere with germination or seedling growth because permeability has been ensured.

The sediment used in the experiments is well-sorted fine sand with a median diameter d_{50} of 0.245 mm; the measured density of sediment grains, ρ_s , and the porosity, ϵ , of the sand are 2.6 g/cm³ and 0.4, respectively.

2.1 Horizontal Bed Experiments

The first part of the experimental campaign has been carried out on a horizontal seabed, where the bottom shear stress at the surface of the consolidated sand has been estimated using existing wave boundary layer models. In the wave flume, two concrete blocks with a triangular geometry and 1/3 slope (Figure 1) have been positioned at a distance of 2 m from each other. The blocks are 0.3 m high, 0.9 m long, and as wide as the width of the flume. The 2-m gap between the blocks has been filled with sand. One wave gauge (WG1) has been located near the wave generator and three wave gauges (WG2–WG4) have been used to evaluate the wave conditions over the horizontal seabed and to separate incident and reflected waves in the wave flume (Figure 1). The bed profile has been observed with a laser profiler for an extension of 1.5 m on the seabed to avoid the edge effects due to the slopes; the area on which the nanosilica has been sprayed is marked with the yellow line in Figure 1. The bottom profile measurement corresponds to the origin of the onshore coordinate x and the water level defines the origin along the vertical axis z . Six regular and six irregular non-breaking wave tests have been conducted. Table 1 lists the incident wave characteristics on Horizontal bottom with Consolidated sand (HC1-12 tests) used in the present study. The listed tests are defined by water depth at the sand bottom, h , wave height, H , wave period, T , and duration, d . For irregular waves, H and T are replaced by the root-mean-square wave height, H_{rms} , calculated as $H_{rms}=H_{m0} / \sqrt{2}$ with H_{m0} = significant wave height and peak period, T_p .

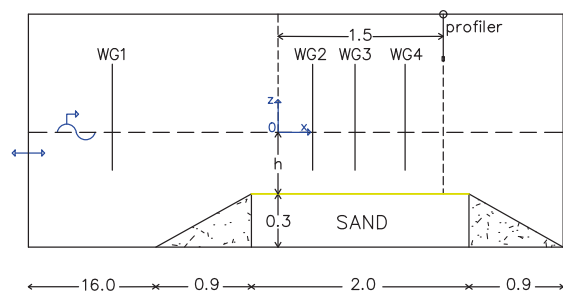


Figure 1: Side view of the experimental setup of Horizontal Consolidated (HC) bottom tests

2.2 Dune Erosion Experiments

In the second part of the experimental campaign, a beach-dune system model has been considered; the cross-shore beach-dune profile has a length of 6.9 m. The beach has a slope of 1/10 on an extension of 5.2 m and a slope of 1/50 on an extension of 0.2 m. The seaward slope of the dune is 1/1.5 on an extension of 0.5 m. The dune crest length is 0.5 m and the dune height above the toe is 0.35 m. Six wave gauges (WG1-WG6) have been used to measure the free surface elevation in the wave shoaling zone. A side view of the beach-dune system as built with the instrumentation is shown in Figure 2. The origin along the onshore coordinate x is taken at WG1 and the water level defines the origin along the vertical axis z . In Table 2, values of the onshore coordinate x (m) and water depth h (m) below the still water level, SWL, at each of the six WGs are listed.

Table 1: Regular and irregular wave characteristics for HC1-12

Test name	Wave type	h [m]	H/H_{rms} [m]	T/T_p [s]	d [s]
HC1	Regular	0.40	0.118	1.00	180
HC2	Regular	0.40	0.141	1.20	216
HC3	Regular	0.50	0.160	1.80	324
HC4	Regular	0.50	0.227	2.00	360
HC5	Regular	0.60	0.209	1.80	324
HC6	Regular	0.60	0.231	2.19	396
HC7	Irregular	0.40	0.069	1.48	8145
HC8	Irregular	0.40	0.085	1.80	2574
HC9	Irregular	0.50	0.108	2.02	2460
HC10	Irregular	0.50	0.134	2.46	1752
HC11	Irregular	0.60	0.133	2.15	1606
HC12	Irregular	0.60	0.150	2.42	1752

The cross-shore profile of the beach-dune system has been measured with the laser profiler in the zone of noticeable profile changes $x = 11.0$ m – 12.5 m (1.5 m onshore distance) with a spatial resolution of sampling interval $\Delta x = 0.002$ m. Seven wave conditions have been considered in water depth of 0.53 m. Tables 3 and 4 list the irregular incident wave characteristics on the beach-dune system defined by H_{rms} and T_p . Starting from time $t = 0$, the initial profile has been exposed to four

runs composed of 230, 230, 330, and 330 waves, respectively. Tests DN1-7 (Dune Natural) refer to a condition of sand without nanosilica and tests DC1-7 (Dune Consolidated) refer to a condition with nanosilica. The nanosilica-based grout has been sprayed in tests DC1-7 from the toe up to the crest of the dune to evaluate the increase of the erosion resistance exclusively on the dune face (yellow line in Figure 2).

Table 2: Onshore coordinate x and water depth h below SWL at WG1-WG6 for dune erosion experiments

WG	WG1	WG2	WG3	WG4	WG5	WG6
x [m]	0	0.4	0.9	7.0	7.3	7.7
h [m]	0.53	0.53	0.52	0.44	0.41	0.38

3 NUMERICAL MODEL

The cross-shore model CSHORE was developed initially to predict the cross-shore transformation under irregular nonlinear waves (Johnson and Kobayashi, 1999). The present version of

Table 3: Irregular wave characteristics in water depth of 0.53 m for DN1-7 with 4 runs

Test name	Run	H/H_{rms} [m]	T/T_p [s]	d [s]
DN1	1	0.071	1.17	252
DN1	2	0.074	1.14	506
DN1	3	0.069	1.19	859
DN1	4	0.069	1.19	1217
DN2	1	0.082	1.56	309
DN2	2	0.081	1.56	617
DN2	3	0.081	1.57	1056
DN2	4	0.081	1.54	1496
DN3	1	0.083	1.99	384
DN3	2	0.083	1.99	768
DN3	3	0.083	2.16	1322
DN3	4	0.083	2.27	1874
DN4	1	0.087	2.49	427
DN4	2	0.087	2.45	862
DN4	3	0.086	2.55	1485
DN4	4	0.086	2.53	2116
DN5	1	0.110	1.23	271
DN5	2	0.109	1.23	542
DN5	3	0.106	1.19	926
DN5	4	0.107	1.19	1313
DN6	1	0.133	1.52	318
DN6	2	0.133	1.52	636
DN6	3	0.130	1.52	1087
DN6	4	0.129	1.54	1539
DN7	1	0.133	1.99	392
DN7	2	0.133	1.99	776
DN7	3	0.131	2.27	1334
DN7	4	0.131	2.27	1890

CSHORE includes various capabilities added for the last 20 years. Theoretical aspects are reported in detail in the CSHORE manual (Johnson et al., 2012) and the later updates are summarized in Kobayashi (2016). The components of CSHORE for normally incident waves and alongshore uniformity include: a combined wave and current model based on time-averaged continuity, momentum, wave energy or action, and roller energy equations; a sediment transport model for bed load and suspended load coupled with the bottom sediment continuity equation. In the present numerical study, the input data include the measured incident wave characteristics from wave probes and the sand bottom elevation z_b from the bed profiler system.

3.1 Sediment Transport

The cross-shore suspended sediment transport rate q_s is expressed as:

$$q_s = a_x \bar{U} V_s \quad 1$$

where a_x = empirical suspended load parameter with a typical value of $a_x = 0.2$ on a gentle slope; \bar{U} = cross-shore return (undertow) current; V_s = suspended sediment volume per unit horizontal area caused by wave breaking and bottom friction. The cross-shore bedload transport rate q_b is expressed as:

$$q_b = \frac{bP_b}{g(s-1)} \sigma_U^3 G_s \quad 2$$

where b = empirical bedload parameter with a typical value of 0.002; P_b = sediment movement probability; g = gravitational acceleration; s = sediment specific gravity; σ_U = standard deviation of the oscillatory depth-averaged velocity U ; G_s = bottom slope function for the bed load, where $G_s = 1$ on the horizontal bottom.

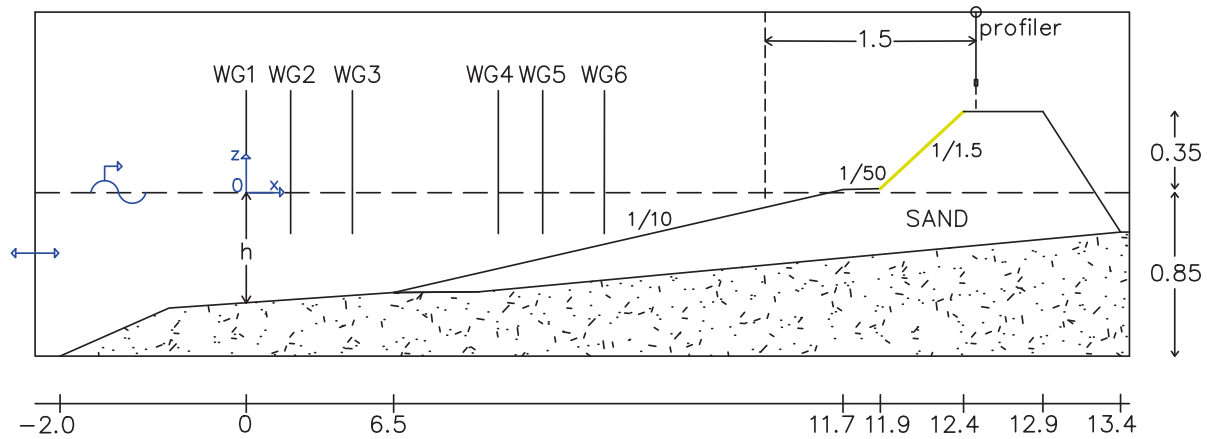


Figure 2: Side view of the experimental setup of Natural and Consolidated Dune (DN and DC) tests

Table 4: Irregular wave characteristics in water depth of 0.53 m for DC1-7 with 4 runs

Test name	Run	H/H_{rms} [m]	T/T_p [s]	d [s]
DC1	1	0.074	1.17	252
DC1	2	0.074	1.20	505
DC1	3	0.071	1.19	855
DC1	4	0.071	1.19	1209
DC2	1	0.082	1.56	311
DC2	2	0.082	1.56	618
DC2	3	0.081	1.57	1053
DC2	4	0.081	1.53	1487
DC3	1	0.086	1.99	369
DC3	2	0.086	2.02	738
DC3	3	0.085	2.21	1266
DC3	4	0.085	2.21	1796
DC4	1	0.088	2.42	429
DC4	2	0.087	2.42	863
DC4	3	0.086	2.47	1485
DC4	4	0.086	2.47	2106
DC5	1	0.107	1.23	274
DC5	2	0.107	1.23	544
DC5	3	0.105	1.19	926
DC5	4	0.103	1.19	1310
DC6	1	0.143	1.53	321
DC6	2	0.143	1.53	641
DC6	3	0.139	1.54	1095
DC6	4	0.138	1.56	1549
DC7	1	0.147	1.99	389
DC7	2	0.147	1.99	773
DC7	3	0.147	1.99	1321
DC7	4	0.141	1.99	1869

3.2 Sediment Transport

In the present study, the nanosilica-based grout of a finite thickness is modeled like a consolidated cohesive bottom containing cohesionless sediment (Kobayashi and Zhu, 2020). The unknown variables are the upper elevation z_p

(t, x) of the consolidated sand layer protecting underneath loose sand and the upper elevation z_b (t, x) of loose sand released after the erosion of the consolidated sand layer. The loose sand layer thickness h_p (t, x) on the consolidated layer is given by:

$$h_p(t, x) = [z_b(t, x) - z_p(t, x)] \quad 3$$

where z_b (t, x) and z_p (t, x) vary with time t and onshore coordinate x . In Figure 3, the unknown variables z_b and z_p are sketched for HC (Figure 1) and DC (Figure 2) tests involving consolidated sand by nanosilica-based grout. At the beginning of each test (time $t = 0$) there is no loose sand and $z_b = z_p$. After the wave attack (time $t = d$), a loose sand layer is formed and $z_b > z_p$ and $h_p > 0$.

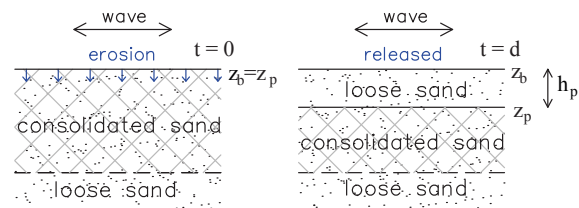


Figure 3: Loose sand upper elevation z_b and consolidated sand upper elevation z_p

The abrasive or protective effect of loose sand released from eroded consolidated sand is considered empirically through the dimensionless function F in terms of the sand movement probability P_b and sand layer thickness h_p :

$$F = (1 + C_a P_b h_*) e^{(-C_p h_*)} ; h_* = \frac{h_p}{d_{50}} \quad 4$$

where C_a = abrasion coefficient; C_p = protection coefficient; h_* = normalized sand layer thickness relative to the median sand diameter d_{50} . Kobayashi and Zhu (2020) calibrated $C_a = 2$ and $C_p = 0.5$ for glacial till. The temporal and cross-shore variations of vertical erosion depth $E(t, x)$ is related to the consolidated sand surface erosion as:

$$E(t, x) = [z_p(t=0, x) - z_p(t, x)] \quad 5$$

Assuming $z_p = z_b$, $h_p = 0$ in Eq.(3) at $t=0$, whereas $E = 0$ at $t = 0$ in Eq.(5).

3.3 Consolidated Sand Erosion

The consolidated sand layer is characterized by the erosion resistance parameter R_c expressed in m^2 / s^2 . The erosion work rate is represented by the product of the resistance force and the vertical erosion rate as:

$$\rho R_c \frac{\partial E}{\partial t} = D \quad 6$$

where ρR_c is the resistance force of the consolidated sand layer per unit horizontal area, ρ is the fluid density and D is the energy dissipation rate per unit horizontal area required for this erosion work (Kobayashi and Weitzner, 2015). The consolidated sand is expressed by the resistance parameter R_c and sand volume fraction f_c . The loose sand released from the consolidated sand is represented by the median diameter d_{50} , porosity n_p , fall velocity w_f and specific gravity s . The loose sand is transported as bed load and suspended load [Eqs.(1) and (2)]. The energy

dissipation rate D is related to the turbulence generated by wave energy dissipation as:

$$D = (e_B D_B + e_f D_f) G_d(S_b) \quad 7$$

where D_B and D_f are the rates of wave energy dissipation per unit horizontal area due to wave breaking and bottom friction, respectively; e_B and e_f are the efficiencies for wave breaking and bottom friction, respectively; G_d is a function of the bottom slope S_b ($G_d = 1$ for $S_b = 0$), introduced to increase erosion on a steep dike slope.

$e_B = 0.0002$ and $e_f = 0.01$ were calibrated by Kobayashi and Weitzner (2015). By substituting Eq.(7) into Eq.(6) and including Eq.(4) for the effect of abrasion or protection of the released loose sand on the consolidated sand layer, the consolidated sand erosion model is summarized as:

$$\rho R_c \frac{\partial E}{\partial t} = F(e_B D_B + e_f D_f) G_d(S_b) \quad 8$$

The conservation equation of loose sand volume per unit horizontal area on the consolidated sand surface is expressed as:

$$(1 - n_p) \frac{\partial h_p}{\partial t} + \frac{\partial}{\partial x} (q_b + q_s) = f_c \frac{\partial E}{\partial t} \quad 9$$

where n_p = the porosity of loose sand taken as 0.4; q_b and q_s are the cross-shore bed load and suspended load transport rates per unit width given by Eq.(1) and Eq.(2); f_c is the sand volume per unit volume of consolidated sand in the range of $0 \leq f_c < (1 - n_p) = 0.6$.

For natural wet sand containing 9.2% clay (Zhu and Kobayashi, 2021), the upper and lower limits of R_c have been estimated as:

$$R_c < 1 m^2 / s^2 \quad 10$$

$$R_c > (1 - n_p) (s - 1) g d_{50} \sim 0.002 m^2 / s^2$$

4 COMPARISON WITH EXPERIMENTS

4.1 Calibration of R_c with the Horizontal Bed Experiment

The estimate of R_c has been performed using observations from the horizontal bed experiment and analytical solutions. In HC tests with non-breaking waves and a horizontal bed, $D_B = 0$ and $G_d = 1$ in Eq.(8). The initial condition of no loose sand on the consolidated sand layer ($h_p = 0$) implies $F = 1$ (no abrasion, no protection) in Eq.(4). Eq.(8) can be simplified as:

$$\rho R_c \frac{\partial E}{\partial t} = e_f D_f \quad 11$$

CSHORE assumes the Gaussian distribution of the depth-averaged horizontal velocity u for random waves (Kobayashi et al., 2007) with \bar{u} = mean related to wave-induced currents and σ_u = standard deviation related to oscillatory wave velocity. The time-averaged wave energy dissipation rate D_f is expressed in terms of \bar{u} and σ_u as:

$$D_f = \frac{1}{2} \rho f_b \sigma_u^3 G_3(u_*) \quad ; \quad u_* = \frac{\bar{u}}{\sigma_u} \quad 12$$

where f_b is the bottom friction factor. Function G_3 can be estimated as $G_3 = |\bar{u}|^3 / \sigma_u^3 = 2\sqrt{2/\pi} = 1.6$ assuming $\bar{u} = 0$ for the horizontal bed experiment. For regular waves, the time-dependent wave velocity can be expressed as $u(t) = U_w \cos(\omega t)$ and $\sigma_u = U_w / \sqrt{2}$ and $G_3 = (8\sqrt{2}) / (8\pi) = 1.2$. Integrating Eq.(11) with Eq.(12) from $t = 0$ to $t = d$:

$$R_c E = \frac{1}{2} e_f f_b G_3 d \sigma_u^3 \quad \text{at } t = d \quad 13$$

where E is the erosion depth at $t = d$ and σ_u is constant during $t = 0 - d$. Velocities have not been measured during the HC tests. One way to estimate σ_u is to assume linear wave theory locally. For linear progressive waves with no setup ($\bar{\eta} = 0$) and no mean velocity ($\bar{u} = 0$), the

standard deviation σ_u of the depth-averaged velocity can be expressed as a function of the free surface standard deviation σ_η (Kobayashi, 2016):

$$\sigma_u = C \frac{\sigma_\eta}{h} \quad 14$$

The standard deviation σ_η is estimated as $\sigma_\eta = H/\sqrt{8}$ for regular wave height H . For irregular waves, $\sigma_\eta = H_{rms} / \sqrt{8}$ with H_{rms} = root mean square wave height.

For the regular wave tests HC1-6 with a horizontal bed, the standard deviation σ_u may be expressed using the horizontal velocity U_w above the bottom boundary layer instead of Eq.(14) for the depth-averaged velocity:

$$\sigma_u = \frac{U_w}{\sqrt{2}} \quad ; \quad U_w = \frac{\pi H}{T \sinh(kh)} \quad 15$$

where $T = 2\pi/\omega$ is the wave period, ω is the angular frequency, and k is the wave number. In Table 5, σ_u and $R_c E$ in Eq.(13) are listed together with the wave characteristics for regular wave tests with consolidated sand. The test duration d is 180-396 s. The difference of σ_u is less than 30% except for HC1, which reaches 50% because of the small wave period. The depth-averaged σ_u in Eq.(14) is larger than the near-bed σ_u in Eq.(15) as expected. The calibration of R_c for HC1-6 is performed by comparing the calculated erosion E using $\sigma_u = C\sigma_\eta / h$ for both regular and irregular waves. The observed erosion E_o may have been 1 mm or less because the consolidated sand appeared intact. In Figure 4, E for regular waves with $R_c = 0.1, 1$ and $10 \text{ m}^2 / \text{s}^2$ is compared with $E_o = 10^{-3} \text{ m}$. The calculated E using $R_c E$ in Table 5 is less than 10^{-3} m (1 mm) for $R_c = 1 \text{ m}^2 / \text{s}^2$ or larger for regular waves.

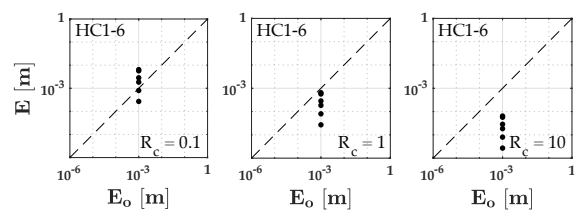


Figure 4: E for regular waves for $R_c = 0.1, 1$ and $10 \text{ m}^2 / \text{s}^2$ in comparison with $E_o = 10^{-3} \text{ m}$

In Table 6, $\sigma_u = C\sigma_\eta/h$ and $R_c E$ are listed together with the wave characteristics for irregular wave tests. The test duration d is 1752-8145 s. In Figure 5, E for irregular waves is compared with $E_o = 10^{-3}$ m in the same way as in Figure 4.

The comparison between E_o and E values in Figures 4 and 5 indicates that R_c is of the order of $1 \text{ m}^2/\text{s}^2$ for the consolidated sand used in this study. In the following computations, $R_c = 1 \text{ m}^2/\text{s}^2$ will be used as the erosion resistance parameter.

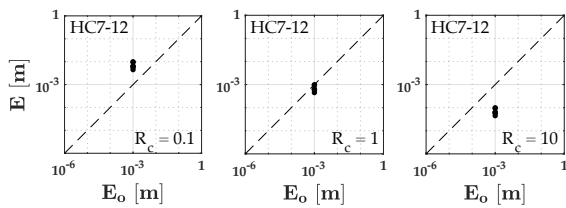


Figure 5: E for irregular waves for $R_c = 0.1$, 1 and $10 \text{ m}^2/\text{s}^2$ in comparison with $E_o = 10^{-3} \text{ m}$

4.2 Incident Wave Characteristics

The wave characteristics used as input in the CSHORE computations are summarized in Tables 1, 3 and 4, assuming $H_{rms} = H_{m0}/\sqrt{2}$ for irregular waves. Incident wave conditions for each test are specified at the seaward boundary location at $x=0$ in Figures 1 and 2. The bottom elevation change and erosion depth of the consolidated sand are computed in the computation domain $0 \leq x \leq x_m$ ($x_m = 1.5 \text{ m}$ in Figure 1 and $x_m = 12.5 \text{ m}$ in Figure 2) for the duration of $0 \leq t \leq d$ where the test duration d has been about one hour for DN and DC tests.

4.3 Comparison with HC Tests

Calculations for the horizontal bed with a consolidated sand case (HC1-12) have been conducted assuming $z_b = z_p$ at $t = 0$ and using standard values of input parameters and $f_c = 0.599$ in Eq.(9). For the HC tests, the computational domain has been restricted to the area in which bed profiles have been observed with the laser profiler. The origin of the domain corresponds to the up-wave boundary of the observation area extending 1.5 m landward along

the x-axis as shown in Figure 1. Figure 6 shows the computed H or H_{rms} , h_p/d_{50} and E at the end of the test duration ($t = d$) for $x = 0 - 1.5 \text{ m}$ for HC5 (regular wave) and HC10 (irregular wave). The wave height decreases landward because of the bottom friction. The loose sand thickness h_p normalized by the median sand diameter d_{50} increases landward because of onshore loose sand transport on the consolidated sand. The deposited sand ($h_p > d_{50}$) reduces the consolidated sand erosion. As a result, E decreases landward. Figure 7 summarizes h_p/d_{50} and E for HC1-6 (regular waves) and HC7-12 (irregular waves). The maximum computed erosion in HC tests is less than about 2 mm, consistent with Figures 4 and 5.

4.4 Cross-Shore Wave Transformation on a Sloping Beach

For the beach-dune system in the DN and DC tests, the initial profiles with a spatial resolution of sampling interval $\Delta x = 0.002 \text{ m}$ (as acquired from the bed profiler system) have been smoothed to $\Delta x = 0.01 \text{ m}$ to reduce measurement fluctuations of about 1 mm. The smoothing did not change the beach and dune profile specified as the initial profile for the CSHORE computations.

The hydrodynamics in the surf zone and the associated sediment transport depend on the process of wave breaking. The crudest assumption is that the ratio of wave height and still water depth is constant throughout the surf zone, $H_{m0}(x)/h(x) = \gamma$, where γ is the breaker ratio parameter. In CSHORE, the parameter γ is used to estimate the local depth-limited wave height required for the rate D_B of breaking wave energy dissipation. In the present study, a typical value of $\gamma = 0.7$ has been increased to obtain a better agreement. In Figures 8 and 9, the measured and computed values of H_{m0} and the mean free surface elevation $\bar{\eta}$ for all runs of tests DN3 and DN5 are compared for $\gamma = 0.7, 0.8$ and 0.9 . The origin of $x = 0$ and the locations of the six wave gauges are shown in Figure 2. The two tests chosen for the calibration of γ have a different hydrodynamic behavior due to different wave conditions: DN3 is characterized by a larger wave period and a lower wave height than DN5 (Table 3).

Table 5: σ_u and $R_c E$ for regular wave tests HC1-6

					$\sigma_u = \frac{U_w}{\sqrt{2}} \text{ [m/s]}$		$\sigma_u = C \frac{\sigma_\eta}{h} \text{ [m/s]}$	
	h [m]	H/H_{rms} [m]	T/T_p [s]	d [s]	σ_u [m/s]	$R_c E$ [m ³ /s ³]	σ_u [m/s]	$R_c E$ [m ³ /s ³]
HC1	0.40	0.118	1.00	180	0.057	3.07E-06	0.118	2.66E-05
HC2	0.40	0.141	1.20	216	0.106	2.33E-05	0.160	7.95E-05
HC3	0.50	0.160	1.80	324	0.154	1.07E-04	0.185	1.85E-04
HC4	0.50	0.227	2.00	360	0.235	4.21E-04	0.271	6.43E-04
HC5	0.60	0.209	1.80	324	0.169	1.42E-04	0.214	2.85E-04
HC6	0.60	0.231	2.19	396	0.219	3.75E-04	0.252	5.70E-04

Table 6: σ_u and $R_c E$ for irregular wave tests HC7-12

	h [m]	H_{rms} [m]	T_p [s]	d [s]	σ_u [m/s]	$R_c E$ [m ³ /s ³]
HC7	0.40	0.069	1.48	8145	0.086	6.26E-04
HC8	0.40	0.085	1.80	2574	0.113	4.50E-04
HC9	0.50	0.108	2.02	2460	0.129	6.40E-04
HC10	0.50	0.134	2.46	1752	0.166	9.68E-04
HC11	0.60	0.133	2.15	1606	0.144	5.74E-04
HC12	0.60	0.150	2.42	1752	0.166	9.65E-04

In the DN3 test computations, wave breaking occurs between $x = 9$ m and $x = 10$ m, the increase of γ shifts wave breaking and wave height decay farther landward. In the shoaling zone, where WG4-6 have been placed (Figure 2), H_{m0} is little affected by changes in γ , therefore the agreement is similar for $\gamma = 0.7 - 0.9$. In the DN5 test, $\gamma = 0.7$ underestimates the wave height: for this reason, γ is taken as 0.9 in the present computations. The computed $\bar{\eta}$ is negative (wave setdown) in the wave breaking zone for $\gamma = 0.7, 0.8$ and 0.9 for test DN3 and slightly negative (wave setdown) for $\gamma = 0.8$ and 0.9 for test DN5. The agreement appears to be good because the measurements have been limited to the zone with a negligible $\bar{\eta}$ (less than 1 mm). It is noted that the profile measurement has been limited to the zone with $x > 11$ m.

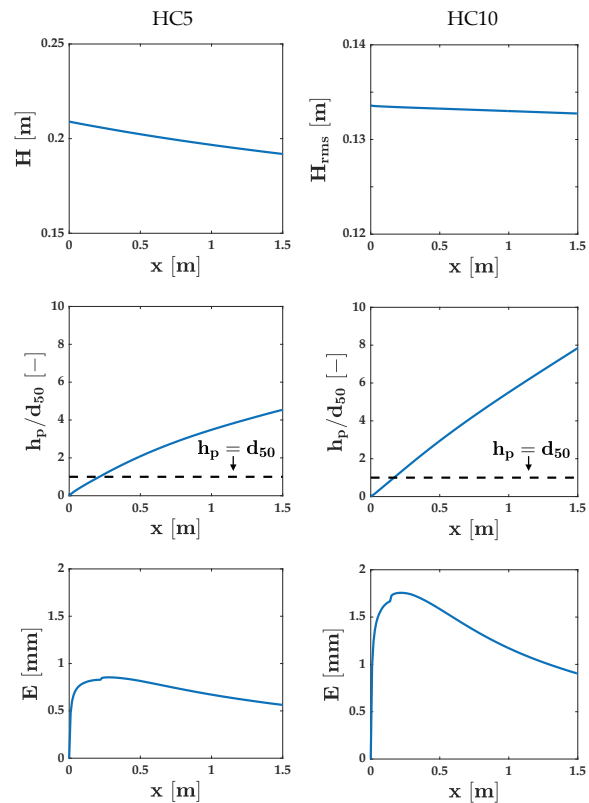


Figure 6: H or H_{rms} , h_p/d_{50} and E at $t=d$ for $x=0-1.5$ m for HC5 (regular wave) and HC10 (irregular wave)

4.5 Comparison with Natural Sand Dune DN Tests

For a steep dune as in Figure 2, the bottom slope function G_s in Eq.(2) exceeds the upper limit of 10 in the form of $|G_s| \leq 10$ as default in CSHORE. A calibration for DN tests has

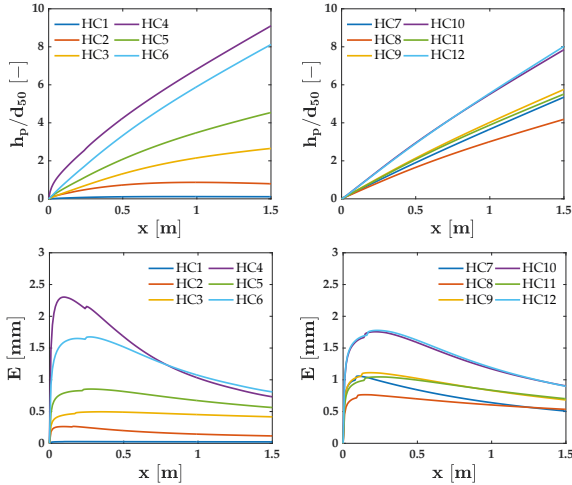


Figure 7: h_p/d_{50} and E at $t=d$ for $x=0-1.5$ m for HC1-6 (regular waves) and HC7-12 (irregular waves)

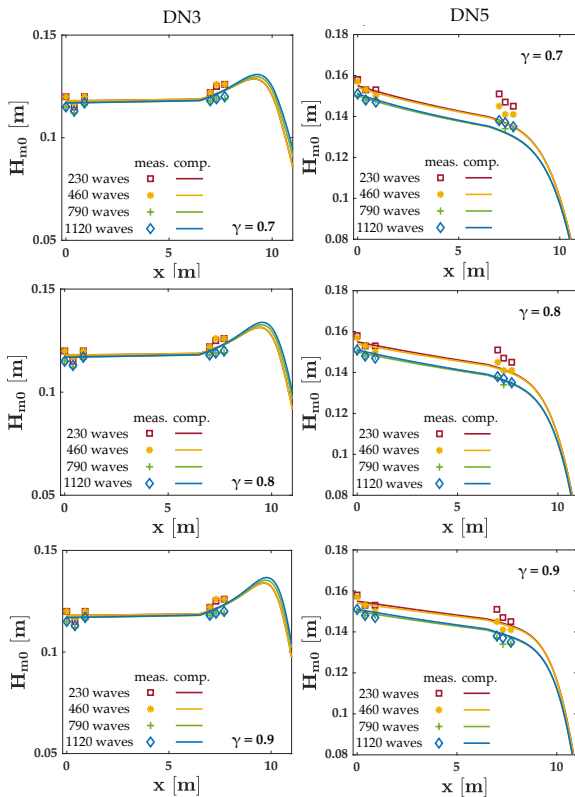


Figure 8: Comparison between measured and computed H_{m0} along x -axis for DN3 and DN5 for breaker ratio parameter = 0.7, 0.8 and 0.9 (irregular waves)

been carried out with respect to the upper limit G_s (GSLMAX) using standard values of the bed load parameter (BLP), suspended load parameter (SLP), suspension efficiency e_f due to bottom friction (EFFF) and suspension efficiency e_b due to wave breaking (EFFB) listed in Table 7; GSLMAX has been increased up to 150 to increase the erosion of the dune slope (1/1.5).

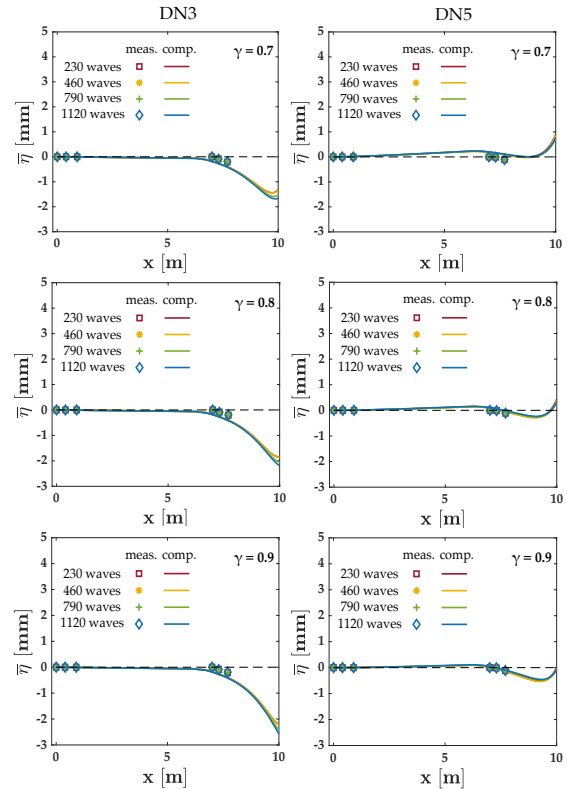


Figure 9: Comparison between measured and computed $\bar{\eta}$ along x -axis for DN3 and DN5 for breaker ratio parameter = 0.7, 0.8 and 0.9

The degree of agreement between the computed and measured profiles is quantified through the calculation of the Root Mean Square Error (RMSE) and the Brier Skill Score (BSS). The BSS compares model performance to a baseline prediction (most commonly “no change”), with a value of 1 representing the perfect agreement of the model predictions with observational data (Sutherland et al., 2004). The BSS applied to the prediction of beach erosion during a wave attack can be presented as:

$$BSS = 1 - \frac{\sum (|z_o - z_m|)^2}{\sum (|z_o - z_b|)^2}$$

Table 7: CSHORE input parameters

Category	Parameters	Value	Description
Wave transformation	Δx	0.01 m	Cross-shore nodal spacing
	γ	0.9	Breaker ratio parameter
	f_b	0.015	Sand bottom friction factor
	$\tan\phi$	0.63	Sediment limiting slope
Sediment transport	BLP	0.002	Bed load parameter
	SLP	0.2	Suspended load parameter
	EFFF	0.01	Suspension efficiency due to bottom friction
	EFFB	0.005	Suspension efficiency due to wave breaking
Sand in experiments	d_{50}	0.24 mm	Median sand diameter
	ω_f	3.4 cm/s	Fall velocity
	s	2.6	Specific gravity
	n_p	0.4	Porosity of sand

where z_o is the cross-shore bed elevation observed post-wave attack, z_m is the final modelled bed level and z_b is the initial (i.e., pre-wave attack) bed elevation. It is noted that the BSS becomes unreliable for tests with little bed elevation changes ($z_o \approx z_b$). For the evaluation of the RMSE and BSS, the entire computation domain has been considered. Table 7 summarizes all the input parameters and the characteristics of sand.

Figure 10 shows the comparison between measured and computed profiles of DN6 and DN7 as a function of GSLMAX together with the calculated RMSE and BSS. Table 8 lists the results for all computations of DN tests. The selection of GSLMAX is performed by evaluating the sum of RMSE and BSS. GSLMAX = 100 minimizes the RMSE and maximizes the BSS.

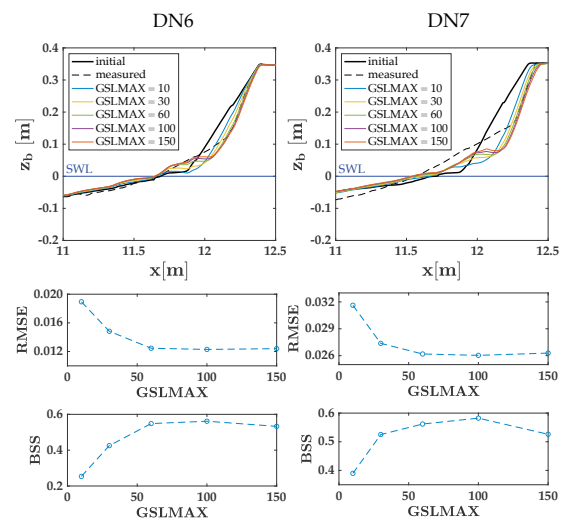


Figure 10: Measured and computed profiles of DN3 and DN7 for GSLMAX = 10, 30, 60, 100 and 150

4.6 Comparison with Consolidated Sand Dune DC 330 Tests

In beach-dune system tests with consolidated sand (DC1-7), computations have been performed with different bottom characteristics along the cross-shore distance in terms of R_c and f_c to reproduce the experimental conditions in the DC tests. In Figure 11, a sketch of numerical domain division is shown; from $x = 0$ to $x = 11.9$ m, values of $R_c = 1000 \text{ m}^2 / \text{s}^2$ and $f_c = 0$ are assumed, for the fixed bottom elevation and practically no erosion (Kobayashi and Weitzner, 2015). A layer of loose sand is placed over the fixed bottom from $x = 6.5$ m up to $x = 11.9$ m to reproduce the experimental setup in Figure 2. Values of $R_c = 1 \text{ m}^2 / \text{s}^2$ and $f_c = 0.599$ are assumed on the dune face from $x = 11.9$ m up to the crest at $x = 12.5$ m where the nanosilica-based grout has been injected. Use is made of the standard values of BLP, SLP, EFFB and EFFF (Table 7) and the calibrated value of $\text{GSLMAX} = 100$ for DN tests. The calibrated value of R_c ($1 \text{ m}^2 / \text{s}^2$) for HC1-12 tests is evaluated for DC tests in the range of $R_c = 0.1\text{-}10 \text{ m}^2 / \text{s}^2$. Figure 12 shows the comparison between the measured and computed profiles of DC5 and DC6 tests for $R_c = 0.1, 1$ and $10 \text{ m}^2 / \text{s}^2$

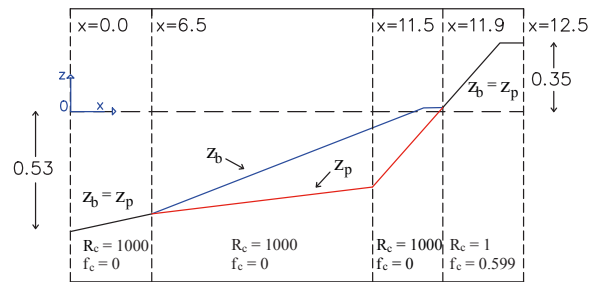


Figure 11: Sketch of numerical domain division for DC1-7 at $t = 0$

together with the obtained RMSE and BSS. Table 9 summarizes the results in terms of RMSE and BSS for all computations of DC tests. The profile changes are relatively small for DC1-7 and BSS defined by Eq.(16) may not be a good indicator for the degree of agreement. It is worth noting that in DC1 the difference between the 3 values of R_c is negligible. For DC2-5, $R_c = 1 \text{ m}^2 / \text{s}^2$ or $R_c = 10 \text{ m}^2 / \text{s}^2$ yields reasonable agreements. In tests DC6 and DC7, the consolidated sand has been eroded at time $t = d$ and $R_c = 0.1 \text{ m}^2 / \text{s}^2$ produces a slight dune erosion and a better agreement.

Table 8: RMSE (m) and BSS for DN tests as a function of GSLMAX

RMSE [m]						BSS [-]					
GSLMAX	10	30	60	100	150	GSLMAX	10	30	60	100	150
DN1	0.012	0.011	0.010	0.009	0.010	DN1	0.00	0.04	0.08	0.12	0.11
DN2	0.017	0.016	0.015	0.010	0.013	DN2	-0.23	-0.14	-0.03	0.09	0.08
DN3	0.026	0.024	0.022	0.021	0.021	DN3	0.13	0.23	0.36	0.43	0.41
DN4	0.055	0.053	0.052	0.045	0.048	DN4	0.06	0.12	0.17	0.23	0.22
DN5	0.012	0.011	0.010	0.009	0.010	DN5	0.05	0.07	0.08	0.09	0.10
DN6	0.019	0.015	0.012	0.012	0.012	DN6	0.25	0.43	0.55	0.56	0.53
DN7	0.032	0.027	0.026	0.026	0.026	DN7	0.39	0.53	0.56	0.58	0.53
Sum	0.172	0.157	0.148	0.133	0.140	Sum	0.65	1.27	1.77	2.11	1.98

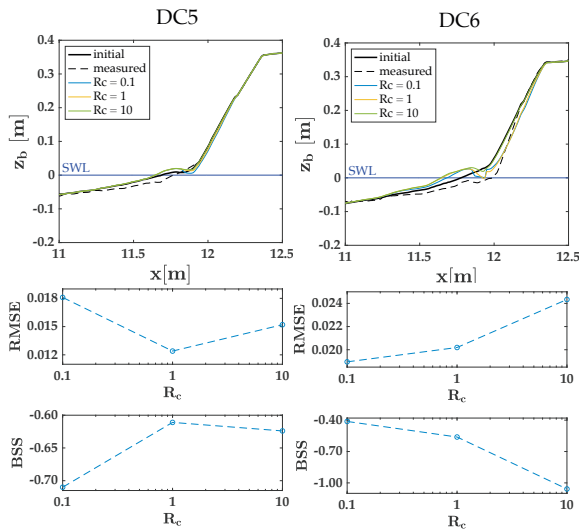


Figure 12: Measured and computed profiles of DC5 and DC6 as a function of $R_c = 0.1, 1$ and $10 \text{ m}^2 / \text{s}^2$

Table 9: RMSE (m) and BSS for DC tests as a function of R_c (m^2 / s^2)

RMSE [m]				BSS [-1]			
R_c	0.1	1	10	R_c	0.1	1	10
DC1	0.011	0.010	0.010	DC1	-0.30	-0.28	-0.30
DC2	0.014	0.012	0.013	DC2	-0.66	-0.41	-0.41
DC3	0.023	0.021	0.022	DC3	-0.83	-0.41	-0.42
DC4	0.028	0.026	0.027	DC4	-0.17	0.20	0.16
DC5	0.018	0.012	0.015	DC5	-0.71	-0.61	-0.62
DC6	0.019	0.020	0.024	DC6	-0.42	-0.55	-1.08
DC7	0.022	0.026	0.027	DC7	-1.30	-2.02	-2.12
Sum	0.135	0.128	0.139	Sum	-4.40	-4.09	-4.80

5 CONCLUSIONS

The cross-shore numerical model CSHORE has been extended to incorporate the erosion process of a consolidated sand layer with a finite thickness above the loose sand. Observations from the small-scale experiments on the horizontal bottom of consolidated sand under regular and irregular

non-breaking waves have been used to estimate analytically the erosion resistance parameter R_c for the limited erosion case of the consolidated sand. The numerical model has been used to examine the process of the consolidated sand erosion, transport and deposition of the horizontal bottom (HC tests). A value of $R_c = 1 \text{ m}^2 / \text{s}^2$ has predicted erosion rates consistent with the experimental observations. Then, computations of irregular wave transformation and dune erosion for DN tests under irregular breaking waves have been carried out for the beach profile with a dune. The beaker ratio parameter used to estimate the local depth-limited wave height required for the rate of breaking wave energy dissipation has been increased by about 30 % to reproduce the measured wave height variation. In addition, the bottom slope function used in the estimation of cross-shore bed load transport rates has exceeded the upper limit of 10 as default in CSHORE; therefore, a calibration based on the statistical error estimation methods has been performed, resulting in the upper limit increase by a factor of 10 for the steep (1/1.5) slope of the dune whose toe is above the SWL.

After reaching a fair agreement with natural sand dune DN tests, computations have been carried out for the consolidated sand dune DC tests using $R_c = 1 \text{ m}^2 / \text{s}^2$, calibrated for the horizontal tests, and $R_c = 0.1 \text{ m}^2 / \text{s}^2$ and $R_c = 10 \text{ m}^2 / \text{s}^2$. For five tests with practically no erosion under wave action lasting about one hour, use of $R_c = 1 \text{ m}^2 / \text{s}^2$ gives results in fair agreement with the observed data. On the other hand, for two tests with noticeable erosion, $R_c = 0.1 \text{ m}^2 / \text{s}^2$ produces a slight erosion of the consolidated sand on the dune face. The detailed cross-shore variation of dune erosion has been difficult to reproduce consistently. Furthermore, the strength of the consolidated sand has not been measured for HC and DC tests. The erosion resistance of the consolidated sand might have varied somewhat for the horizontal bed and steep dune tests. A further calibration of CSHORE has to be done with field data for this purpose. A method has to be developed for quantifying the erosion resistance of sand reinforced by nanosilica-based grout at a field site.

Use of nanosilica can be assumed as a nature-based solution to reinforce vulnerable sand dunes

that will be exposed to future sea level rise and storm intensification.

ACKNOWLEDGMENTS

The present study has been partially supported by the Regione Puglia through the grant project titled “Sperimentazione di tecnologie innovative per il consolidamento di dune costiere (INNO-DUNECOST)”, POR Puglia FESR FSE 2014-2020-Sub-Azione 1.4.B, Contract n. RM5UKM2.

Author Contributions: Conceptualization and supervision, N.K. and G.R.T.; numerical simulations, E.L.; data analysis and curation, writing-original draft preparation, E.L.; review and editing, N.K. F.D. and G.R.T. All authors have read and agreed to the published version of the manuscript.

REFERENCES

- D’Alessandro F. and Tomasicchio G.R. (2016). Wave–dune interaction and beach resilience in large-scale physical model tests. *Coastal Engineering*, 116: 15–25.
- D’Alessandro F., Tomasicchio G.R., Francone A., Leone E., Frega F., Chiaia G., Saponieri A., and Damiani L. (2020). Coastal sand dune restoration with an eco-friendly technique. *Aquatic Ecosystem Health & Management*, 23 (4): 417–426.
- Foti E., Musumeci R. E. and Stagnitti M. (2020). Coastal defence techniques and climate change: A review. *Rendiconti Lincei. Scienze Fisiche e Naturali*, 31 (1): 123–138.
- Johnson B. D., and Kobayashi N. (1999). Nonlinear time-averaged model in surf and swash zones. *Coastal engineering 1998*, 2785–2798.
- Johnson B. D. Kobayashi N., Gravens M. B. et al. (2012). Cross-shore numerical model CSHORE for waves, currents, sediment transport and beach profile evolution. *Rep. No. ERDC/CHL TR-12-22, U.S. Army Corps of Engineers, Coastal and Hydraulics Lab.*
- Kobayashi N. (2016). Coastal sediment transport modeling for engineering applications. *Journal of Waterway, Port, Coastal, and Ocean Engineering*, 142 (6): 03116001. American Society of Civil Engineers.
- Kobayashi N., Gralher C. and Do K. (2013). “Effects of woody plants on dune erosion and overwash.” *Journal of Waterway, Port, Coastal, and Ocean Engineering*, 139 (6): 466–472.
- Kobayashi N., Meigs L. E., Ota T. and Melby J. A. (2007). Irregular breaking wave transmission over submerged porous breakwater. *Journal of waterway, port, coastal, and ocean engineering*, 133 (2): 104–116.
- Kobayashi N. and Weitzner H. (2015). Erosion of a seaward dike slope by wave action. *Journal of Waterway, Port, Coastal, and Ocean Engineering*, 141 (2): 04014034.
- Kobayashi N. and Zhu T. (2020). Erosion by wave action of consolidated cohesive bottom containing cohesionless sediment. *Journal of Waterway, Port, Coastal, and Ocean Engineering*, 146 (2): 04019041.
- Leone E., Kobayashi N., Francone A., De Bartolo S., Strafella D., D’Alessandro F. and Tomasicchio G. R. (2021). Use of nanosilica for increasing dune erosion resistance during a sea storm. *Journal of Marine Science and Engineering*, 9 (6): 620.
- Nairn R. B. and Southgate H. N. (1993). Deterministic profile modelling of nearshore processes. Part 2. Sediment transport and beach profile development. *Coastal Engineering*, 19 (1-2): 57–96.
- Sutherland J., Peet A. and Soulsby R. (2004). Evaluating the performance of morphological models. *Coastal engineering*, 51 (8-9): 917–939.
- Todaro C. (2021). Grouting of cohesionless soils by means of colloidal nanosilica. *Case Studies in Construction Materials*, 15: e00577.
- Tomasicchio G. R., D’Alessandro F. and Barbaro G. (2011). Composite modelling for large-scale experiments on wave–dune interaction. *Journal of Hydraulic Research*, 49 (sup1): 15–19.

Zhu T. and Kobayashi N. (2021). Modeling of soft cliff erosion by oblique breaking waves during a storm. *Journal of Waterway, Port, Coastal, and Ocean Engineering*, 147 (4): 04021009.

